Energy Conversion and Management: X 21 (2024) 100505

Contents lists available at ScienceDirect

Energy Conversion and Management: X

journal homepage: www.sciencedirect.com/journal/energy-conversion-and-management-x

A stochastic variance reduction gradient-based GSO-ANFIS optimized method for maximum power extraction of proton exchange membrane fuel cell

K. Jyotheeswara Reddy [a], Ritesh Dash [a], Vivekanandan Subburaj [b], B. Hemanth Kumar [c], C. Dhanamjayulu [d,*], Frede Blaabjerg [e,*], S.M. Muyeen [f,*]

[a] School of Electrical and Electronics Engineering, REVA University, Benagluru, India
[b] Department of Electrical Engineering NIT, Silchar, India
[c] Department of Electrical and Electronics Engineering, Mohan Babu University, India
[d] School of Electrical Engineering, Vellore Institute of Technology, Vellore, India
[e] Department of Energy, Aalborg University, Aalborg, 9220, Denmark
[f] Department of Electrical Engineering, Qatar University, Doha 2713, Qatar

ARTICLE INFO

Keywords:
Fuel cell
MPPT
GSO-ANFIS
ANN
Optimization

ABSTRACT

Proton Exchange Membrane Fuel Cells (PEMFCs) play a pivotal role in the clean energy landscape, yet their efficiency is contingent upon effective power optimization. This paper presents Maximum PowerPoint Tracking (MPPT) control schemes for PEMFCs, focusing on a ground-breaking methodology. Traditional MPPT controllers are instrumental in maintaining optimal performance; however, they often struggle with dynamic operating conditions. In response to this challenge, this research work presents a pioneering MPPT control scheme employing a stochastic variance reduction gradient system. The novelty of this approach lies in its fusion with the Glow Swarm Optimization (GSO) and the Adaptive Neuro Fuzzy Inference System (ANFIS), resulting in a robust hybrid controller. In the pursuit of optimizing the PEMFC system, the proposed GSO-ANFIS controller is subjected to rigorous testing under dynamic variations in both PEMFC temperature and load. Notably, PEMFCs, due to fluctuations in pressure and temperature, exhibit stochastic behaviour, forming a Gaussian surface. In this research, the popular Perturb and Observe (P&O) and Incremental Conductance methods are evaluated alongside the newly introduced GSO-ANFIS model. The proposed GSO-ANFIS controller outperforms its counterparts, showcasing an impressive accuracy level of 89.97%. In contrast, the Artificial Neural Network (ANN) achieves 80.33% accuracy, and the standalone ANFIS controller attains 86.5% accuracy. This disparity underscores the efficacy and potential of the novel hybrid approach, which not only adeptly handles the stochastic nature of PEMFCs but also significantly enhances accuracy in power optimization. This research not only contributes a valuable addition to the field of MPPT control but also offers a promising trajectory for the future development of efficient and reliable PEMFC systems.

1. Introduction

Energy has become a critical driving force in defining mankind's overall sustainability and growth [1]. Renewable energy sources and energy storage technologies have received widespread attention. Fuel cells (FCs) have been favoured options for decades due to their superior performance over traditional carbon-based power sources [2]. Compared to traditional renewable energy sources like solar and wind, FCs are clean energy-producing units and more efficient [3]. Furthermore, the ease of use and modularity of FCs make them suitable for a wide range of vehicle, maritime, and utility-grid applications. Among all the available FCs, Proton Exchange Membrane Fuel Cells (PEMFC) are more popular due to their operational circumstances, high energy density, quick start-up, and low weight [4].

The PEMFC provides the required power based on several parameters, including hydrogen and oxygen gas pressures, cell temperature, and membrane water content [5]. For constant operating conditions, a PEMFC system can only generate its maximum output at one specific

* Corresponding authors.
E-mail address: fbl@et.aau.dk (F. Blaabjerg).

https://doi.org/10.1016/j.ecmx.2023.100505

Available online 8 December 2023

Table 1
Overview of different MPPT controllers available for PEMFC.

Ref	MPPT Technique	Converter Type	Remarks
[6,7]	P&O	Boost	P&O has low convergence speed and produces oscillations at MPP
[8,9]	IC	Boost	IC results in error tracking, particularly for abrupt changes in operating conditions
[12,13]	FLC	Boost	High memory is needed for FLC and the rules must be manually framed
[14,15]	ANN	High gain boost	To train the system, ANN requires an enormous amount of training data
[18]	ANFIS	High gain boost	A large amount of data is necessary to train ANFIS
[19]	JAYA	Boost	It suffers from sluggish convergence speed and become trapped in local optimal points
[20]	GWO	Boost	Low precision and low convergence are problems for GWO
[21]	PSO	Boost	PSO has a poor rate of convergence
[22]	SSA	Boost	SSA does not adapt well to changes in operating conditions
[23]	ALO	Boost	Effective search space exploration is a challenge for ALO, particularly in multimodal functions when the global optimum is situated in a remote area.
[25]	WSA	Boost	The performance of WCA is sensitive to its parameters. Poorly tuned parameters can lead to inaccurate MPPT tracking
[26]	FA	Boost	FA suffers from slow convergence, especially in high-dimensional search spaces
[29]	CSA	Boost	Finding the ideal balance between exploration and exploitation is a problem in CSA
[30]	BAT	Boost	It is not suitable for dynamic operating conditions

point on the power-current curve, known as the Maximum Power Point (MPP). As a result, the PEMFC system needs a Maximum Power Point Tracking (MPPT) control algorithm to maximize efficiency. This can be accomplished by controlling the duty cycle of the DC-DC boost converter. According to this perspective, designing and creating adequate interfacing MPPT control systems for PEMFCs is a significant and technically difficult task for a variety of PEMFC applications. In the literature, various MPPT controllers are developed for photovoltaic and wind generators. Unlike PV/wind generators, very few MPPT controllers have been reported in the literature for fuel cell systems. An overview of some exemplary studies on FC MPPT techniques is provided below.

The Perturb & Observe (P&O) MPPT technique has been frequently used in the literature for regulating the PEMFC output [7,7]. The P&O can run the PEMFC at its MPP under various operating circumstances. P&O uses fixed step size and generates oscillations at MPP also has poor convergence speed, which increases the energy loss. In [8,9], variable step size MPPT controllers based on Incremental Conductance (IC) and Incremental Resistance (IR) methods have been outlined. In comparison to the P&O approach, IC and IR methods achieved better transient and steady-state responses. In [10], the performance of P&O is compared to that of IC approach employing a DC-DC boost converter-based PEMFC system. The simulation results show that the IC method is more effective than the P&O technique and it has better stability thanks to its minimum oscillations around the MPP. In [11], a fractional order-based IC technique has been developed for the PEMFC system. It has variable step size control and provides several advantages over traditional IC and P&O in steady-state and transient responses.

On the other hand, intelligent control algorithms are introduced to the PEMFC-connected systems to overcome the shortcomings of classical MPPT approaches. In [12,13], Fuzzy Logic Control (FLC) based MPPT control techniques are presented. It has the positives of flexible operation and fast convergence. But, the main drawbacks of an FLC controller are it requires high memory and the rules have to be framed manually. In [14–16], Neural Network (NN) based MPPT controllers are implemented for the PEMFC system. However, this method demands a huge amount of training data to train the system. In [17,18], authors designed an Adaptive Neuro-Fuzzy Inference System (ANFIS) based MPPT controller for PEMFC fed electric vehicle application. Also, the authors tested the performance of the controller for different cell temperatures. ANFIS controller has advantages of both FLC and NN. However, a redundant amount of data set is required for training.

In recent times, various optimization techniques have been proposed to control the PEMFC output. In [19], JAYA optimization technique has been developed for a hybrid PV-PEMFC system. Grey Wolf Optimization (GWO) and Particle Swarm Optimization (PSO) techniques are developed to generate the maximum power from the PEMFC system [20,21]. Besides, Salp Swarm Algorithm (SSA) [22], Ant Lion Optimization (ALO) [23], Sine Cosine Algorithm (SCA) [24], Water Cycle Algorithm (WCA) [25], Firefly Optimization (FO) [26], Elitist Invasive Weed Optimization (EIWO) [27], Eagle Strategy (ES) [28], Cuckoo Search Algorithm (CSA) [29], BAT [30] are recently developed to extract maximum output from PEMFC applications. Table 1 summarizes the various MPPT control techniques available for PEMFC systems and outlines their limitations.

The literature survey above suggests that employing optimized MPPT controllers can increase the complexity of a system's design and implementation due to the utilization of intricate algorithms and control strategies. Consequently, this complexity may lead to an overall rise in the system's cost. Although optimized MPPT controllers can enhance system efficiency and performance, their advantages might not be significant compared to simpler MPPT controllers, especially under dynamic temperature and pressure conditions. Tuning and optimizing these optimized MPPT controllers for specific operational circumstances can be time-consuming and challenging to execute in practice.

This research is motivated by the objective of enhancing the efficiency and reliability of PEMFCs in power generation. PEMFCs play a vital role in clean energy production, but their effectiveness heavily depends on efficient power management, especially when operating conditions fluctuate. Various methods such as ANFIS, ANN, and PSO have been attempted to improve PEMFCs. However, these methods face difficulties in dealing with the unpredictable and constantly changing behavior of fuel cells.

The distinctive feature of the GSO-ANFIS model lies in its innovative strategy. While conventional ANFIS models may struggle to cope with the unpredictable nature of PEMFCs, the GSO-ANFIS model enhances flexibility by incorporating swarm intelligence. This integration enables the model to navigate complex solutions more efficiently. Furthermore, the inclusion of ANFIS equips the system with adaptive learning capabilities, enabling it to adjust to the changing conditions of PEMFCs over time. Unlike ANN, which might encounter challenges in understanding the complex relationships within PEMFC systems, the GSO-ANFIS model provides a more detailed insight.

By combining ANFIS with swarm intelligence, this model can manage the intricate, nonlinear connections inherent in PEMFC behavior. This comprehensive approach empowers the GSO-ANFIS model to outperform traditional ANN models, ensuring accurate predictions and optimization of PEMFC power output. The proposed GSO-ANFIS controller has the following advantages.

- The Proposed GSO-ANFIS MPPT controller has the potential to enhance the efficiency of a PEMFC system by precisely tracking the MPP of the PEMFC, even under dynamic temperature and partial pressure conditions.
- GSO-ANFIS algorithm can achieve rapid and precise convergence to the optimal solution, leading to faster and more dependable MPPT.
- The proposed GSO-ANFIS controller offers a relatively low computational cost in comparison to other optimization techniques, making

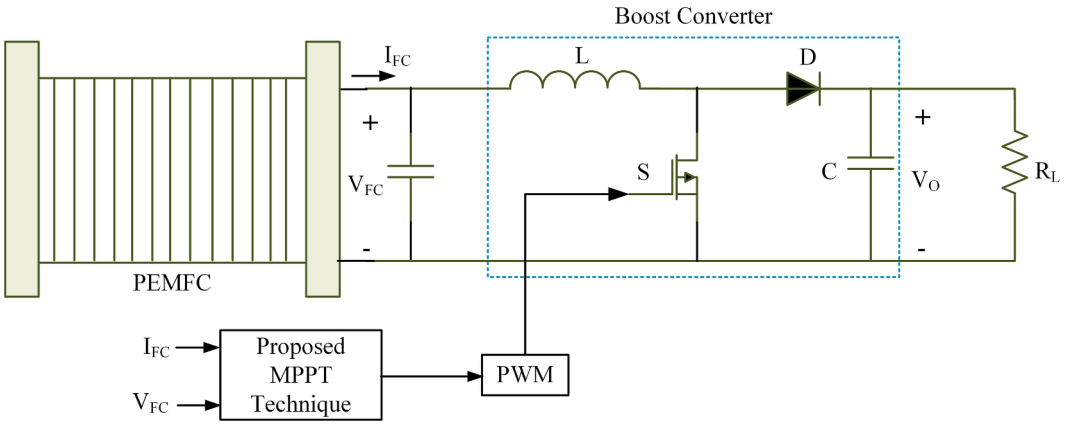

Fig. 1. PEMFC system with MPPT controller.

them suitable for use in low-cost micro-controllers or embedded systems.

The remainder of the document is structured as follows: the subsequent section will delve into system modeling, Section 3 will concentrate on the design of MPPT, Section 4 will present the simulation findings, Section 5 will compare the performance of three MPPT controllers, and the final section will discuss the conclusion.

2. System Modeling

The proposed system depicted in Fig. 1 comprises a 1.2 kW PEMFC stack, a conventional DC-DC boost converter, and an MPPT controller. The current and voltage values of the PEMFC stack are measured and transmitted to the MPPT controller as input signals, which generates an output signal for the PWM generator to operate the converter switch. The converter transforms the input voltage of 24 V into an output voltage of 200 V.

2.1. PEMFC Modeling

PEMFC polarisation curve is nonlinear and highly impacted by operational parameters such as temperature, partial pressures of hydrogen and oxygen gases and membrane water content. The PEMFC output voltage can be calculated taking into account activation loss (V_{Act}), ohmic loss (V_{Ohm}), and concentration loss (V_{Con}) [31].

$$V_{FC} = V_{Nernst} - V_{Act} - V_{Ohm} - V_{Con} \tag{1}$$

Where V_{Nernst} refers to the Nernst voltage or open circuit voltage and it can be determined by using the following equation [32]:

$$V_{Nernst} = 1.229 - 8.5 \times 10^{-4}(T - 298.15) + 4.385 \times 10^{-5} T \cdot ln(P_{H2} + 0.5P_{O2}) \tag{2}$$

where T denotes the temperature in Kelvin. P_{H2} and P_{O2} are hydrogen and oxygen pressure parameters respectively.

The activation loss is calculated by using the following equation:

$$V_{Act} = [\xi_1 + \xi_2 T + \xi_3 T \ln(C_{O2}) + \xi_4 T \ln(I_{FC})] \tag{3}$$

where $\xi_1, \xi_2, \xi_3, \xi_4$ are empirical coefficients, and C_{O2} denotes the concentration of dissolved oxygen in mol/cm^3, which is represented as:

$$C_{O2} = \frac{P_{O2}}{5.08 \times 10^6 \times e^{\frac{-498}{T}}} \tag{4}$$

The value of the ohmic loss is determined by ohmic resistance (R_M) and is determined as follows:

$$V_{Ohm} = I_{FC} \cdot R_M \tag{5}$$

The ohmic resistance of PEMFC can be estimated as following:

$$R_M = \frac{\rho_M l_M}{A} \tag{6}$$

where ρ_M is the membrane resistivity in Ωcm, l_M is membrane thickness in cm and A is the area of PEMFC in cm^2.

The membrane resistivity ρ_M can be determined by using the following equation:

$$\rho_M = \frac{181.6\left[1 + 0.03\left(\frac{I_{FC}}{A}\right) + 0.0062\left(\frac{T}{303}\right)\left(\frac{I_{FC}}{A}\right)^{2.5}\right]}{\left[\lambda_M - 0.634 - 3\left(\frac{I_{FC}}{A}\right)\right] exp\left[4.18\left(\frac{T-303}{T}\right)\right]} \tag{7}$$

where λ_M represents membrane water content. The concentration voltage loss is impacted by the movement of oxygen and hydrogen gases.

$$V_{Con} = -\frac{RT}{nF} ln\left(1 - \frac{I_{FC}}{AI_{max}}\right) \tag{8}$$

where n signifies the number of electrons involved in the reaction and I_{max} denotes current density limiting value in Acm^{-2}. The aforementioned equations were utilized by the authors to build the PEMFC Simulink model.

2.2. DC-DC Boost Converter

In this work, a boost converter operating at 10 kHz switching frequency is intended to step up a PEMFCs 625 V DC voltage to 1.2 kV. A boost converter changes an unstable voltage into a desired voltage by adjusting the proportion of time that the switch is closed and open at a high switching rate. The voltage gain of conventional boost converter is given as follows:

$$\frac{V_0}{V_{FC}} = \frac{1}{1 - D} \tag{9}$$

The selection of components, like the inductor and capacitor, is critical in reducing the ripple content based on switching frequency. The inductance and capacitance values are determined by using the Eqs. 10 and 11.

$$L = \frac{V_{FC}(V_0 - V_{FC})}{\Delta I f_s V_0} \tag{10}$$

$$C = \frac{DI_0}{f_s \Delta V_0} \tag{11}$$

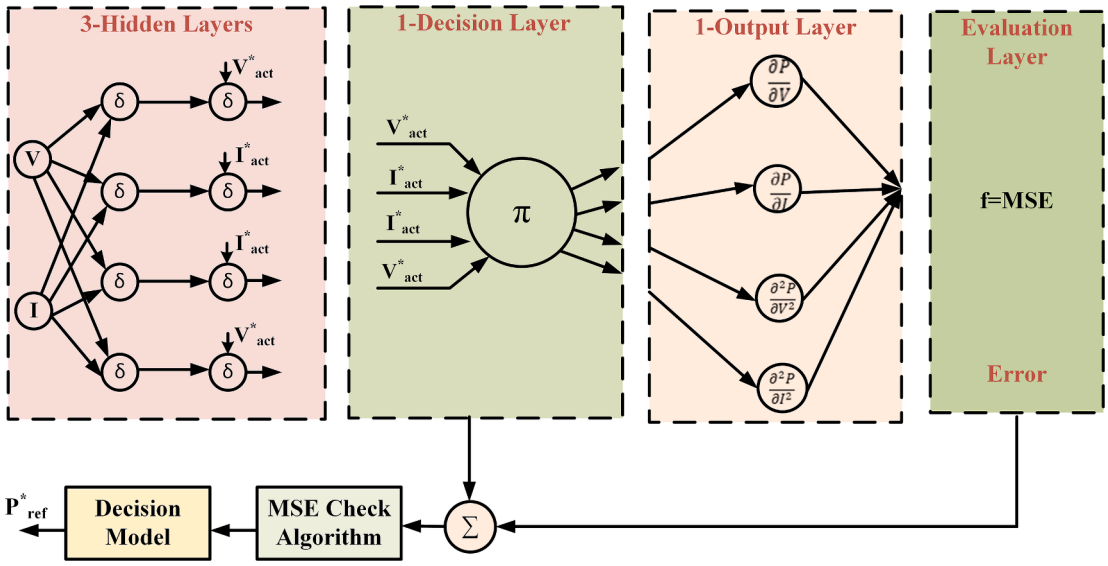

Fig. 2. Three layer analysis of ANN for reference power generation to PI controller.

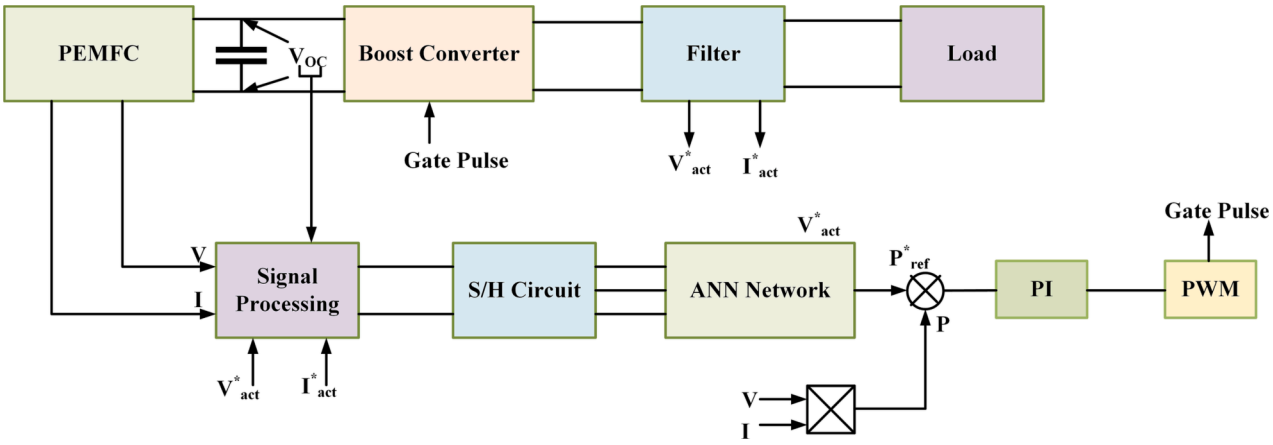

Fig. 3. Block diagram ANN powered MPPT for PEMFC.

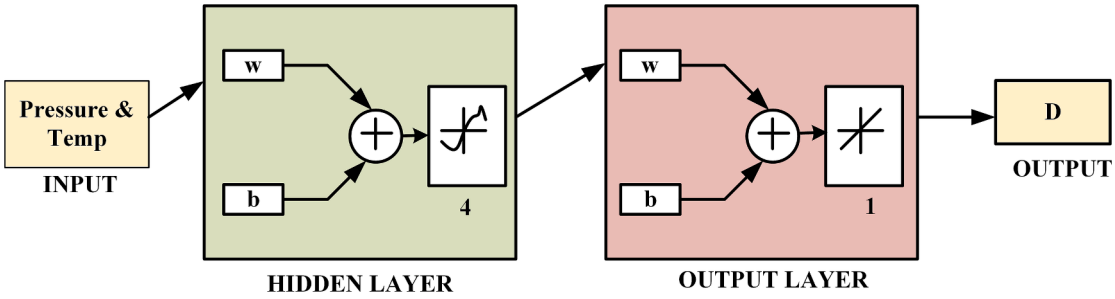

Fig. 4. ANN architecture for four hidden layer mapping from input to output.

3. MPPT

3.1. ANN

An artificial neural network operates based on the principles of a biological neural network. Each neuron in the system is assigned a weight function through linear functional analysis. Non-linear functionality is then applied to each node to evaluate the weighted sum of the average for each neuron. The activation function used is a non-linear activation function that can be calculated as follows:

$$z = \sum_{m=1}^{m} w_m x_m + \alpha \tag{12}$$

In Eq. 12, $x_1, x_2, x_3 \ldots x_m$ represents the input signals and w_m represents the weight of each neuron participating in the function. "α" represents the bias value present in the data for providing necessary correction to the weighted sum error. In the present model, sigmoid activation function has been used as activation function for the non-

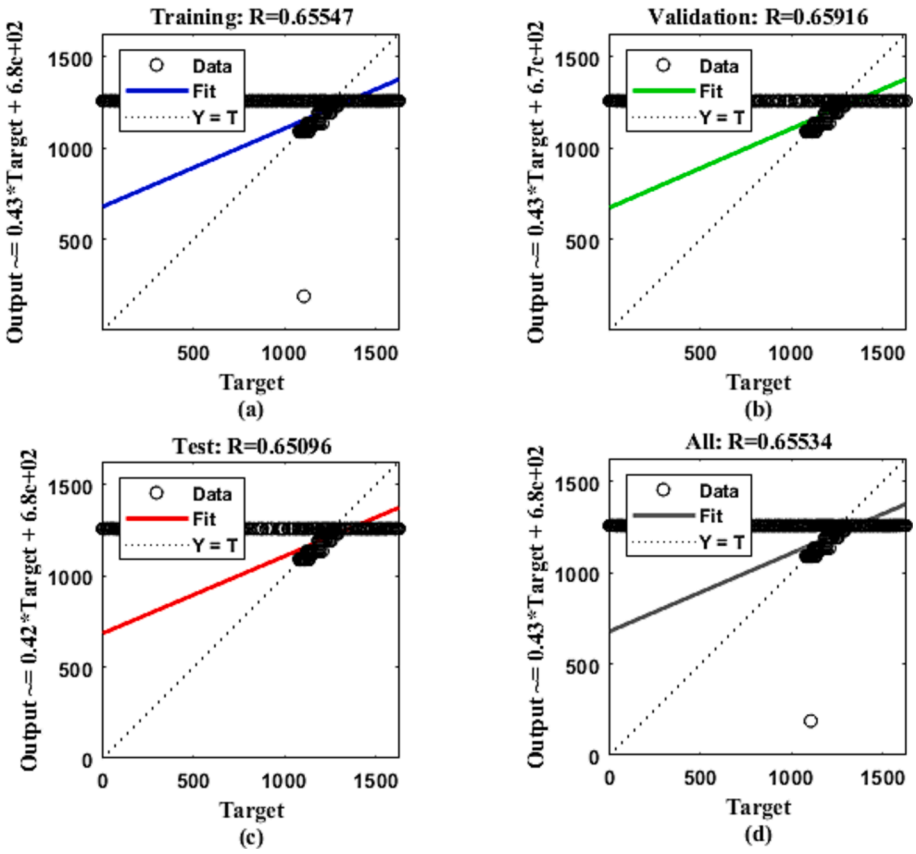

Fig. 5. Curve fitting analysis of data set using ANFIS for forecasting a) epoch = 100 and hidden layer = 5 b) epoch = 110 and hidden layer = 5 c) epoch = 100 and hidden layer = 6 d) epoch = 110 and hidden layer = 6.

Table 2
Progress performance analysis of ANN.

Parameter	Value	Remarks
Epoch	221	Iteration level
Time	0.01	Time for each epoch to get executed
Performance	3×10^5	-
Gradient	8.83×10^5	Vector partial derivative to cost function
mu	0.001	Learning rate to determine step size
Validation check	60%	To check the performance of the each predicted point

linear system analysis.

Fig. 2 depicts a feed-forward neural network with a three-layer architecture: the hidden layer, decision layer, and output layer. The input hidden layer, also known as the buffer layer, distributes inputs such as PEMFC voltage and current based on their respective weight values. The decision layer analyzes the inputs and generates decisions for the reference power generation of the PI controller. The output layer consists of a single neuron that provides these decisions to the PI controller.

Fig. 3 shows the block diagram of an ANN-based MPPT controller for a PEMFC system. The proposed gate signal is generated by the PWM circuit in accordance with the load requirements, as determined by the Levenberg–Marquardt ANN optimization method. During the ANN optimization process, the output gate pulse is a function of the converter output voltage (the target parameter) and the PEMFC voltage and current (the input vector parameters). To improve the accuracy and efficiency of the optimization process, pre-processed training patterns have been applied to the optimization window, thereby reducing the processing and training time required. It is worth noting that having more MPP matching patterns results in a more accurate global MPP optimization system.

Fig. 4 and 5 illustrate the ANN architecture with four hidden layers that map from the input to the output, establishing the relationship between cell temperature and fuel pressure with PWM duty cycle generation. Table 2 presents the performance analysis of the ANN training and testing.

A total 221 numbers of iterations have been carried out to map the input parameters like temperature and pressure with the duty cycle.

3.2. ANFIS

The controller based on Neural Network utilizes two distinct neural network models, one for process dynamics modeling, and the other for control purposes. Each neural network consists of numerous nodes, each having its own weight. As a result, the adaptive neural network control method updates each node and weight at every stage. However, Model-based Predictive Control (MPC) requires significant computational power, which can only be achieved by ensuring a consistent sampling interval. Therefore, the effectiveness of MPC is limited to particular use cases.

As discussed earlier, ANFIS can be employed as a solution to the control problem for a controller application, utilizing a neural network comprising multiple nodes and small weights to design a control architecture. The process of tuning parameters to achieve the optimal solution can be accomplished using the ANFIS concept.

The development of a neuron frequency controller through inverse training can be categorized into two stages: node learning and process application. In the node learning stage, a set of random variables is generated from the initial process and supplied to the controller to generate a test output throughout the system. This also involves the learning of the controller itself. In the process application phase, the

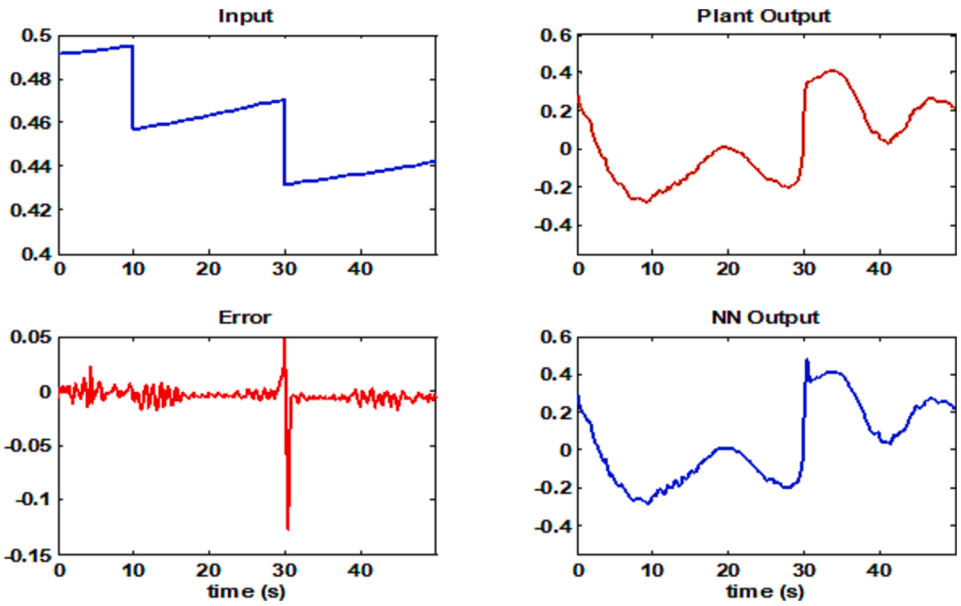

Fig. 6. Validation of data using Neural Network for sample.

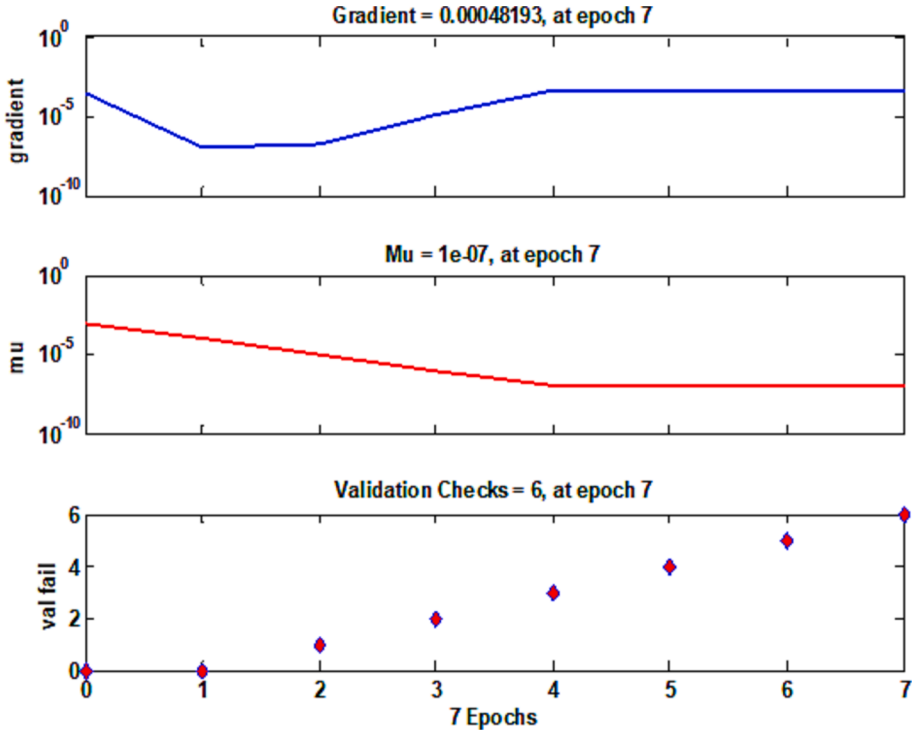

Fig. 7. Neural Network Training State for sample.

identifier is incorporated into the ANFIS-based controller to create the desired output. It is assumed that the learning process is straightforward, resulting in the creation of an inverse plant process to produce the desired output. However, minimizing the error in the network does not necessarily minimize the error in the whole system. The discussed learning process minimizes the error at each node of the system, and therefore, the backpropagation learning method can be employed to reduce the global error in the module. This requires a plant model that is similar to the original plant model or the plant's behaviour for which the controller is being designed. As a result, it is critical to determine the Jacobian parameters for the target plant.

In order to develop an ANFIS controller, input parameters that exhibit linear variation in accordance with process requirements must be selected. Initially, two inputs are chosen to represent the starting condition of the plant output. These inputs are fed into a PI controller, which generates the plant process target. Furthermore, these inputs are employed in the subsequent phases to train the neural network and model replication. The controller utilizes triangular membership functions as parameters for organizing input and output variables, employing five membership functions (NL, NS, ZE, PS, and PL). The control parameters are trained through 10 epochs at each interval during the training phase.

In order to obtain a well-optimized, trained FIS file from ANFIS, it is essential to acquire and validate accurate data with minimal errors. To

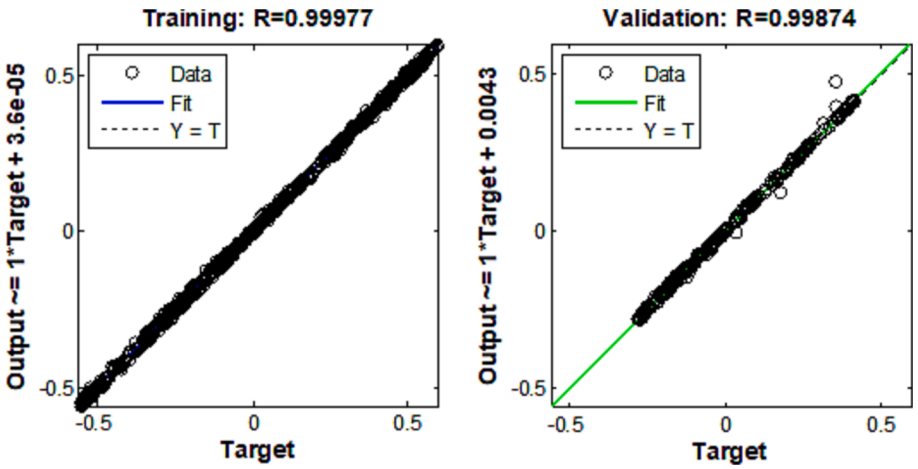

Fig. 8. Neural Network Regression analysis for Sample.

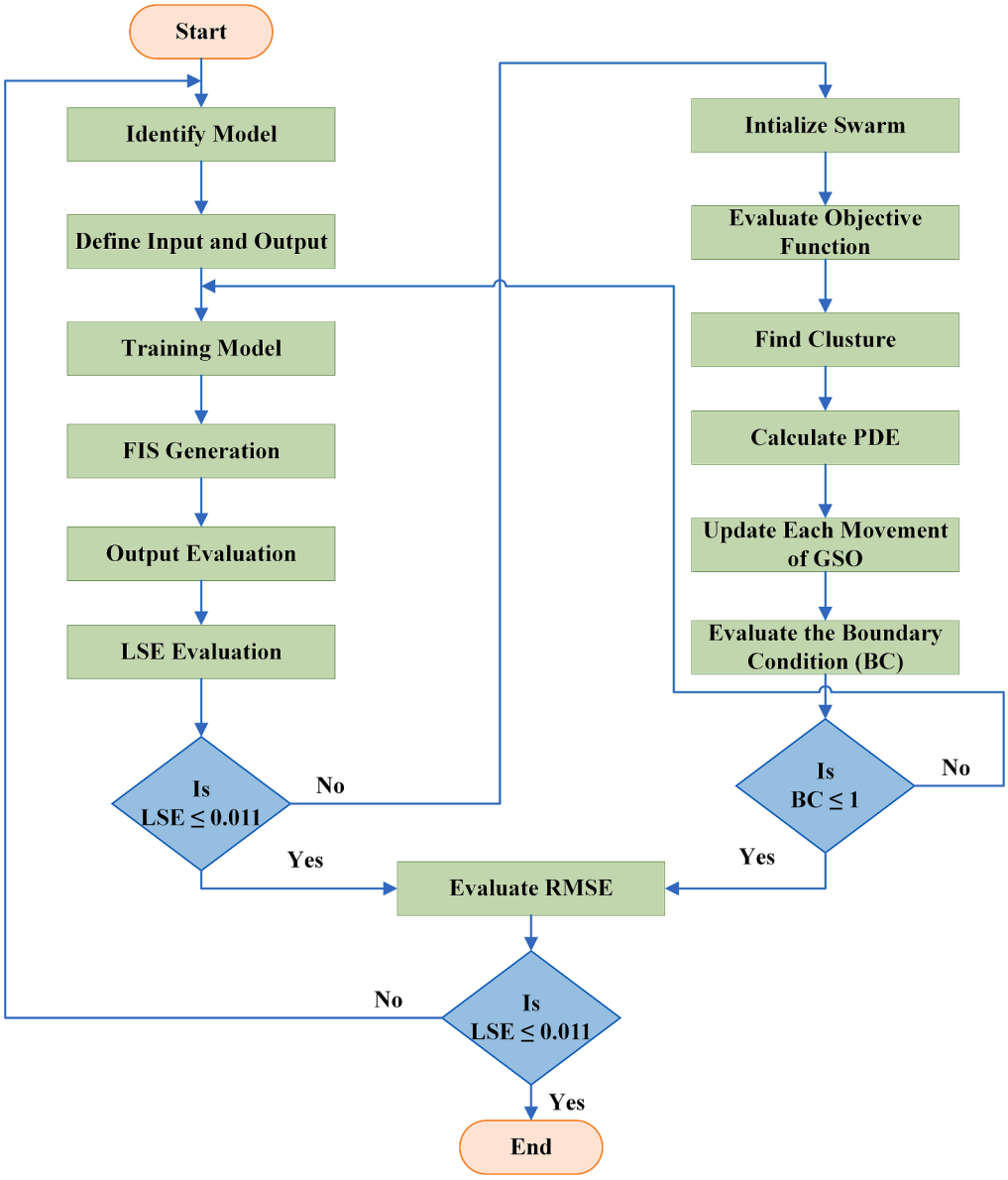

Fig. 9. Flowchart of GSO-ANFIS Controller.

Table 3
The detailed specification of PEMFC used in the MATLAB Simulink model.

Sr. No.	Name of Parameter	Symbol	Magnitude	Unit
1	Slack Power	P	1259.96	Watt
2	Fuel Cell Resistance	R_f	0.061	Ohm
3	Hydrogen Utilization	H_2	99.92	%
4	Oxidant Utilization	O_2	1.81	%
5	Nominal Fuel Consumption		15.22	slpm
6	Nominal Air Consumption		36.22	slpm
7	Exchange Current	I_0	0.027	Amp
8	Exchange Coeffiient	α	0.308	
9	System Temperature	T	328	Kelvin
10	Fuel Supply Pressure	P_{fuel}	1.5	bar
11	Air Supply Pressure	P_{air}	1	bar

Table 4
MATLAB Simulink Boost Converter Parameter

Sr. No.	Parameter	Symbol	Magnitude	Unit
1	Input Voltage	V_{in}	200	V
2	Inductance	L	0.041	H
3	Capacitance	C	$2.76X10^{-4}$	Farady
4	MOSFET Voltage	V_{mosfet}	162	mV
5	Diode Voltage	Dv	0.5	V
6	Duty Cycle	D	0.88	
7	Switching Frequency	F	10 X 10 ^{3}	Hz

achieve this, the data collected from the PI controller is verified using the Neural Network (NN) predictive tool available in MATLAB. This involves extracting the Id and Iq parameters from the input and output of the PI controller to enhance the accuracy of the results.

Fig. 5, shows the Curve fitting analysis of the data set using ANFIS for forecasting a) epoch = 100 and hidden layer = 5 b) epoch = 110 and hidden layer = 5 c) epoch = 100 and hidden layer = 6 d) epoch = 110 and hidden layer = 6. The regression coefficients, R = 0.655 for training and R = 0.659 for validation, provide valuable insights into the model's performance. While these coefficients fall below the ideal value of 1.0, it is important to consider the complexity of the design and the chosen architecture (hidden layer of 6) in the neural network. These coefficients indicate a moderate correlation between the predicted and actual values during both training and validation phases.

The error between the input to output and that of the Neural Network output is displayed in Fig. 6, with transient behaviour observed around 30 s due to a change in load demand. The typical error range falls between −0.012 to 0.012, except during the transient state. The Levenberg–Marquardt algorithm is then employed, resulting in a total performance of 3.92e06 with a gradient of 1.04e-05.

Successful training with a minimum error of 0.01 during the training condition is illustrated in Fig. 6. Fig. 7 shows the neural network training state, including the gradient and Mu. It is apparent from Fig. 7 that a gradient of 0.00048193 is maintained for the training of Id sample-1 at epoch-7. Regression analysis was performed, and the results for R = 0.99977 and R = 0.99874 are shown in Fig. 8.

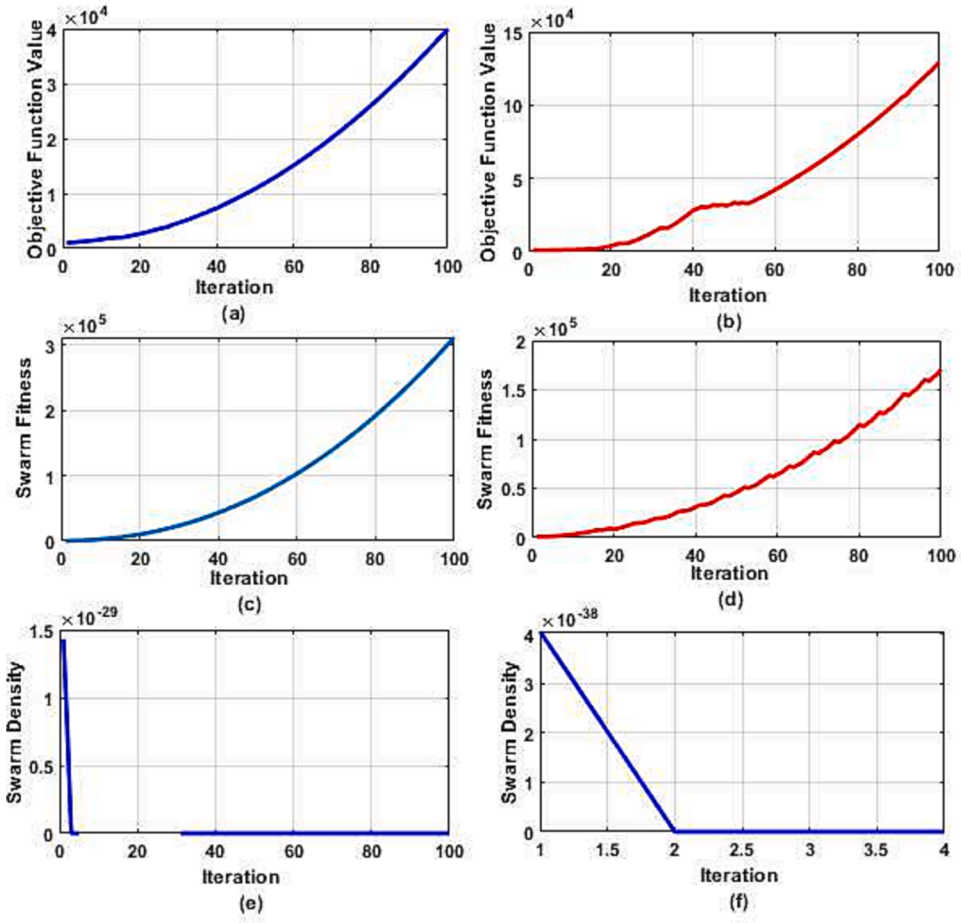

Fig. 10. Performance Analysis of Glow Swarm Optimization with respect to iteration level (a) Objective Function Value vs. Iteration- trajectory (b) Objective Function Value vs. Iteration- actual (c) Swarm Fitness Vs Iteration- trajectory (d) Swarm Fitness vs. Iteration- actual (e) Swarm Density vs. Iteration- trajectory (f) Swarm Density vs. Iteration- actual.

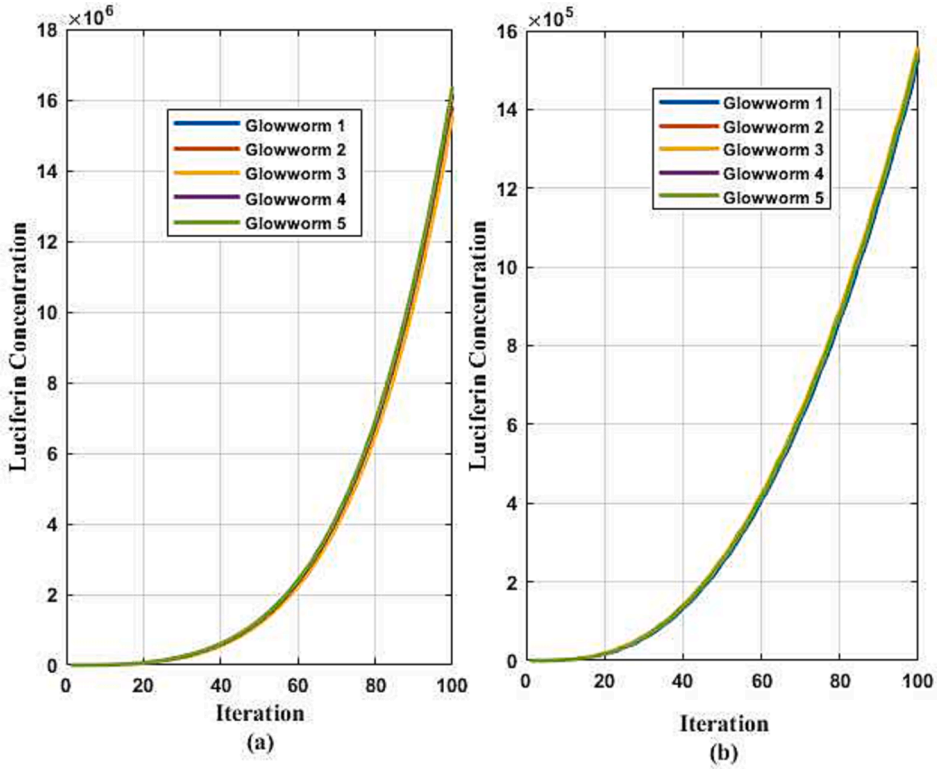

Fig. 11. Luciferin Concentration a) Projected path of attraction b) Actual path of attraction.

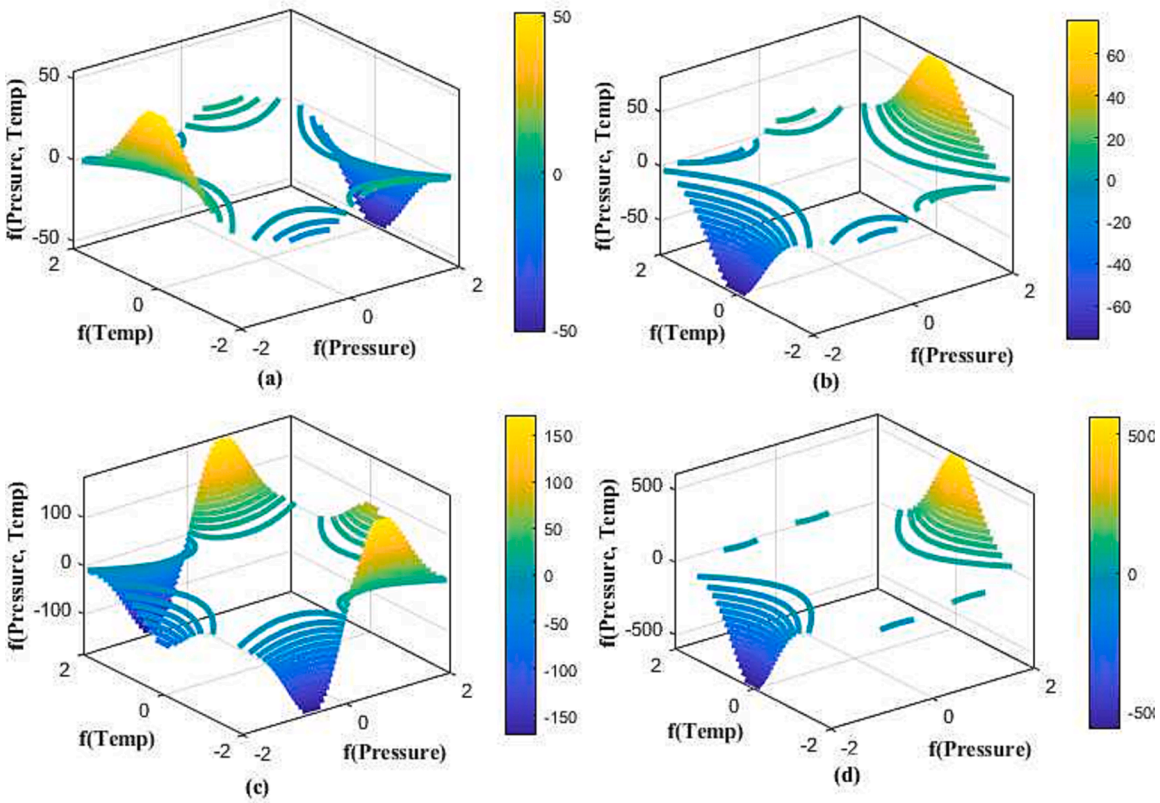

Fig. 12. Search space optimization for GSO + ANFIS model a)λ =0.22 and β =0.53 b)λ =0.27 and β =0.48 c) λ =0.29 and β =0.44 d) λ =0.31 and β =0.53.

Table 5
Performance comparison of proposed GSO-ANFIS with the benchmarking model with P&O algorithm.

Type	Model	ANN	ANFIS	GSO-ANFIS
Training Data	MAE	0.299	0.283	0.268
	RMSE	0.368	0.377	0.321
	R-Squared	0.673	0.820	0.584
	Accuracy Rate	77.63	78.01	89.96
Testing Data	MAE	0.307	0.311	0.277
	RMSE	0.366	0.382	0.591
	R-Squared	0.714	0.848	0.631
	Accuracy Rate	83.22	82.99	90.03

Table 6
Performance comparison of proposed GSO-ANFIS with benchmarking model with INC algorithm.

Type	Model	ANN	ANFIS	GSO-ANFIS
Training Data	MAE	0.117	0.147	0.108
	RMSE	0.121	0.135	0.091
	R-Squared	0.781	0.793	0.922
	Accuracy Rate	82.09	89.23	96.11
Testing Data	MAE	0.037	0.149	0.097
	RMSE	0.214	0.217	0.199
	R-Squared	0.781	0.818	0.921
	Accuracy Rate	88.06	93.29	95.62

3.3. GSO + ANFIS Model

GSO is a metaheuristic optimization algorithm inspired by the behaviour of glow-worms. It was first introduced by Krishnanand and Ghose in 2005. The glow-worm swarm optimization algorithm utilizes a group of ”agents” to simulate the actions of individual glow-worms. These agents traverse a search space that mirrors the problem at hand, while following a set of regulations that imitate the glow-worm’s behaviour. Moreover, the agents communicate with each other to accomplish the optimization objective. GSO is a versatile algorithm capable of handling both continuous and discrete optimization problems. Its effectiveness has been demonstrated across a wide range of applications, including but not limited to function optimization, clustering, and wireless sensor network routing.

The GSO-ANFIS model is a fusion optimization approach that blends GSO and ANFIS. ANFIS is an artificial neural network that combines fuzzy logic and neural networks to produce precise decisions or predictions, and it has found wide applications in control systems, data classification, and pattern recognition.

The GSO ANFIS model employs GSO to fine-tune the parameters of the ANFIS model. The GSO algorithm adjusts the input membership functions and output scaling factors of the ANFIS network, leading to an improvement in the model’s prediction accuracy. This hybrid model has shown great potential in solving intricate optimization problems in various domains, including medical diagnosis, power system stability analysis, and time-series prediction, outperforming traditional optimization methods and ANFIS models on several occasions. The flowchart of the GSO-ANFIS Controller is given in Fig. 9.

4. Performance Analysis

In this section, a detailed analysis for the proposed method for maximum power extraction from PEMFC has been presented. Table-3 shows the detailed specification of PEMFC used in the MATLAB simulink model as a case study. Here both fuel and air are supplied at 1.5 and 1 bar respectively.

Similarly, the boost converter parameters are presented in Table-4. The system has been modeled initially for a static type of duty cycle to analyze the result and the latter has been converted into a dynamically changed cycle in accordance with the optimization parameter. The initial duty cycle has been set to 0.88 along with a switching frequency of 10,000 Hz.

The fuel cell has been tested under the variation of temperature and pressure content with the proposed model along with the benchmarking models for evaluating the efficiency of the system.

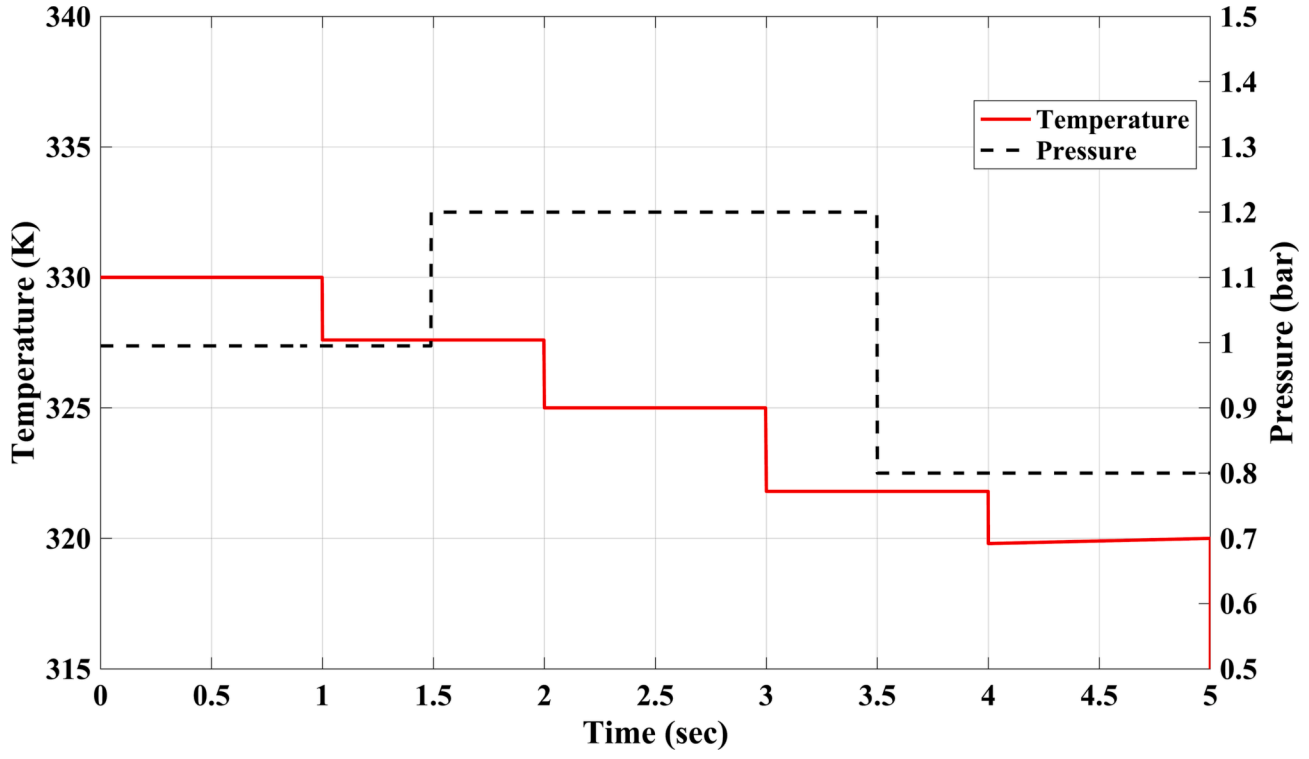

Fig. 13. PEMFC temperature and pressure changes.

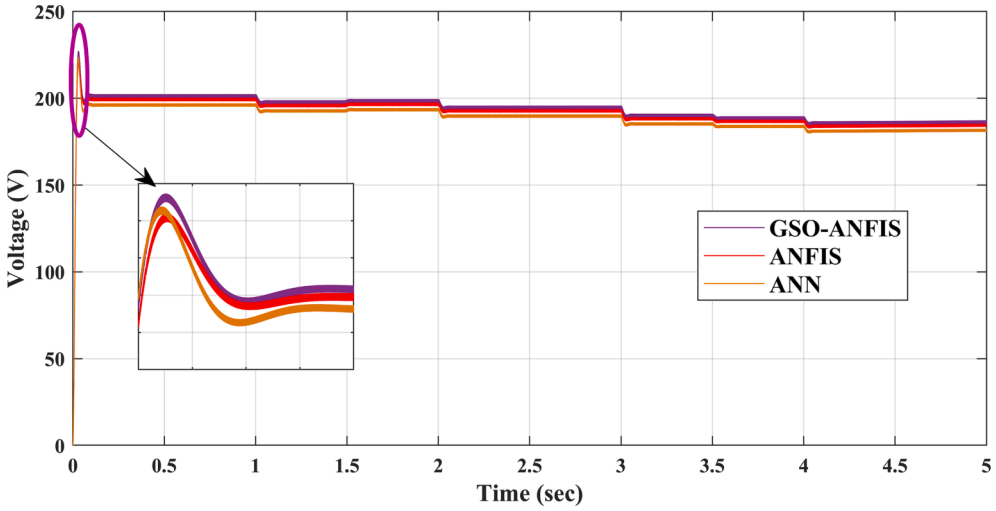

Fig. 14. Comparative analysis of voltage waveform with all controllers.

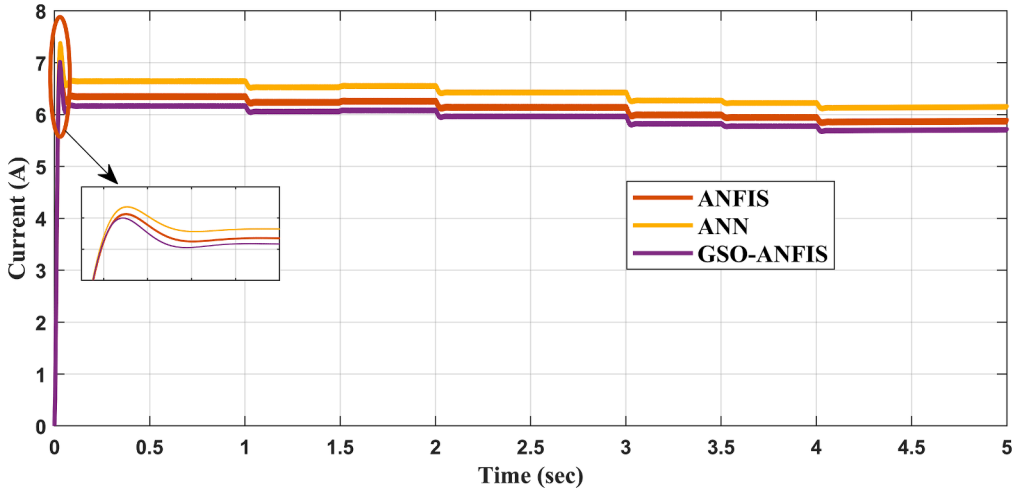

Fig. 15. Comparative analysis of current waveform of with all controllers.

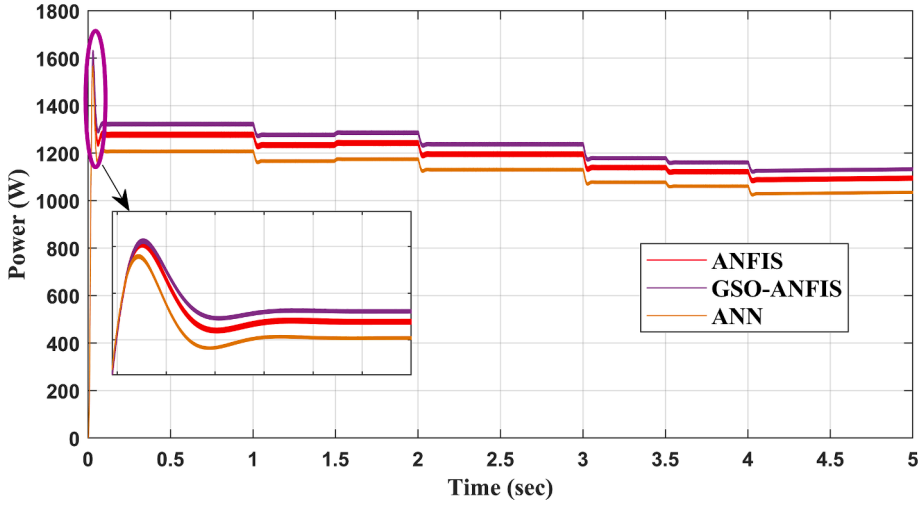

Fig. 16. Comparative analysis of power waveform with all controllers.

Table 7
Comparative analysis of different power quality studies in PEMFC.

Model	Transient Time	di/dt Level	% Change	dv/dt Level	% Change
ANN	t1	0.371	5.81	0.448	6.23
	t2	0.323	4.82	0.39	5.42
	t3	0.206	3.86	0.249	3.46
	t4	0.492	7.34	0.595	8.26
	t5	0.377	5.62	0.456	6.33
	t6	0.364	5.43	0.440	6.11
	t7	0.381	5.83	0.453	6.07
ANFIS	t1	0.342	4.56	0.392	5.44
	t2	0.284	4.01	0.344	4.78
	t3	0.188	2.66	0.228	3.17
	t4	0.423	5.96	0.512	7.11
	t5	0.329	4.63	0.398	5.53
	t6	0.318	4.48	0.385	5.35
	t7	0.332	4.68	0.402	5.58
GSO-ANFIS	t1	0.298	4.20	0.360	5.01
	t2	0.262	3.69	0.317	4.40
	t3	0.174	2.45	0.211	2.93
	t4	0.389	5.47	0.470	6.53
	t5	0.302	4.26	0.366	5.08
	t6	0.293	4.12	0.354	4.92
	t7	0.305	4.30	0.369	3.13

Table 8
Performance comparison of proposed GSO-ANFIS with benchmarking model + P&O algorithm.

Type	Model	ANN	ANFIS	GSO-ANFIS
Training Data	MAE	0.595	0.573	0.552
	RMSE	0.691	0.704	0.626
	R-Squared	1.1115	1.319	0.991
	Accuracy Rate	84.79	85.21	94.88
Testing Data	MAE	0.606	0.612	0.565
	RMSE	0.688	0.710	1.00
	R-Squared	1.172	1.358	1.075
	Accuracy Rate	85.89	85.65	92.91

Table 9
Performance comparison of proposed GSO-ANFIS with benchmarking model + INC algorithm.

Type	Model	ANN	ANFIS	GSO-ANFIS
Training Data	MAE	0.643	0.619	0.596
	RMSE	0.746	0.760	0.676
	R-Squared	1.204	1.425	1.071
	Accuracy Rate	87.34	87.76	98.33
Testing Data	MAE	0.637	0.642	0.593
	RMSE	0.723	0.746	1.051
	R-Squared	1.231	1.426	1.109
	Accuracy Rate	83.68	83.44	90.75

4.1. Case-1:- At dynamic temperature and pressure conditions

To validate the performance of the proposed GSO-ANFIS optimized MPPT model, the fuel cell has been tested under dynamic temperature and pressure conditions using both the benchmarking models and the GSO-ANFIS model. Algorithm 1 presents the pseudo-code for the GSO-ANFIS model, which is used to extract the maximum power from the fuel cell.

Algorithm 1: Pseudo Code for GSO-LSTM MPPT

Require: Initialize GSO parameter, μ, α
Ensure: Ensure Duty Cycle $(D) \geqslant 0.78$
Begin, randomly choose the initial population
Repeat, Evaluate fitness value and MSE for each iteration
for each iteration $i \leqslant N$ **then**

(*continued on next column*)

(*continued*)

Algorithm 1: Pseudo Code for GSO-LSTM MPPT

Compute MSE
if MSE $i_{MSE} < 0.33$
$i_{MSE} = RMSE$
else
$i_{MSE} = i_{MSE} + 0.001$
end if

Based on algorithm-1, the system has been evaluated. Fig. 10 represents the performance analysis of GSO with respect to iteration level. The performance of the objective function for the proposed trajectory and actual value against each epoch level is represented in Fig. 10 and Fig. 10(b) respectively. As can be observed, the MSE for the actual and predicted curves are almost similar up to 20 iterations/epoch level. However, the slope becomes ineffective from 30 to 50 iterations due to a change in the pressure level at the input. Thereafter system follows the desired path. Similarly Fig. 10(b) and Fig. 10(d) show the performance analysis of swarm fitness value with iteration, for both the reference trajectory path and actual trajectory path. The optimization curve exhibits an oscillating behavior throughout the model because each time the optimization window evaluates the error and tries to compensate for it by changing the step size with respect to the R-value.

Fig. 11 illustrates the concentration of luciferin in both projected and actual values for the swarm. In Fig. 11(a), it can be seen that the performance concentration of luciferin is high for all five swarms. This indicates that the optimization ANFIS model will attempt to maintain as many wavelengths (concentration level) as possible during disturbance conditions. Similarly, Fig. 12 represents the search area optimization model for GSO-ANFIS model. It can be observed that the search area shrinks from a higher search space to a lower search space for the same amount of power at a variable rate of $\pm 3di/dt$. This reduction in search time also decreases the complexity involved in the process.

Table 5 and Table 6 presents the performance comparison of the proposed GSO-ANFIS model with benchmarking models with P&O and INC methods. As observed, the GSO-ANFIS model demonstrates higher accuracy rates, specifically 90.03 with P&O and 88.56 with INC. Two statistical analysis with training and testing data has been carried out. The R-square error parameter is notably better for the P&O method compared to the INC method. Consequently, in this results analysis section, the P&O algorithm was used for further efficiency analysis of all benchmarking models and the proposed model.

The performance of the PEMFC system with different control techniques is examined with seven states which are formed by sudden variations in PEMFC temperature and pressure. The variations in the PEMFC parameters (states) are as follows: between 0 and 1 s, the temperature is 338 K and the pressure is 1 bar; between 1 and 1.5 s, the temperature is 327 K and the pressure is 1 bar; between 1.5 and 2 s, the temperature is 327 K and the pressure is 1.2 bar; between 2 and 3 s, the temperature is 325 K and the pressure is 1.2 bar; between 3 and 3.5 s, the temperature is 323 K and the pressure is 1.2 bar; and between 3.5 and 4 s, the temperature is 323 K and the pressure is 0.8 bar; and between 4 and 5 s, the temperature is 320 K and the pressure is 0.8 bar. These variations are illustrated in Fig. 13.

Fig. 14 displays the load voltage waveforms for the proposed model and benchmarking models. It is evident that the proposed model exhibits the least voltage fluctuation during the transient interval compared to the other models. Additionally, the initial voltage peak is lower than that of the ANN and ANFIS models.

The current drawn by the load from PEMFC is shown in Fig. 15. As observed, the maximum current overshoot occurs in ANN controller with untuned system parameters. The proposed GSO-ANFIS controller not only provides better current but also provides improved power performance, as shown in Fig. 16.

Table 7 presents a comparative analysis of different power quality studies in PEMFC. The results show that the maximum rate of change of

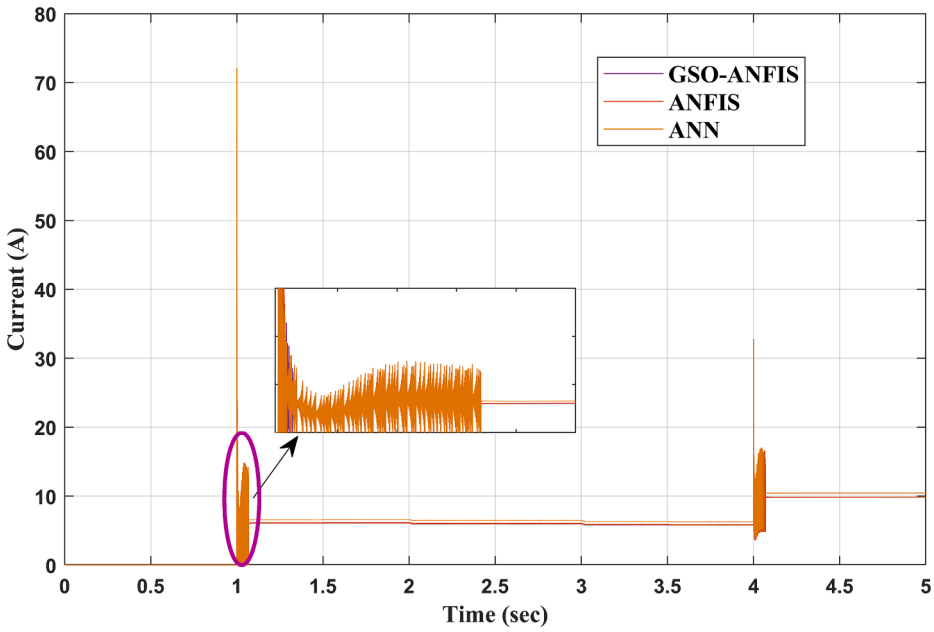

Fig. 17. Comparative analysis of current waveform of all the models under dynamic loading conditions.

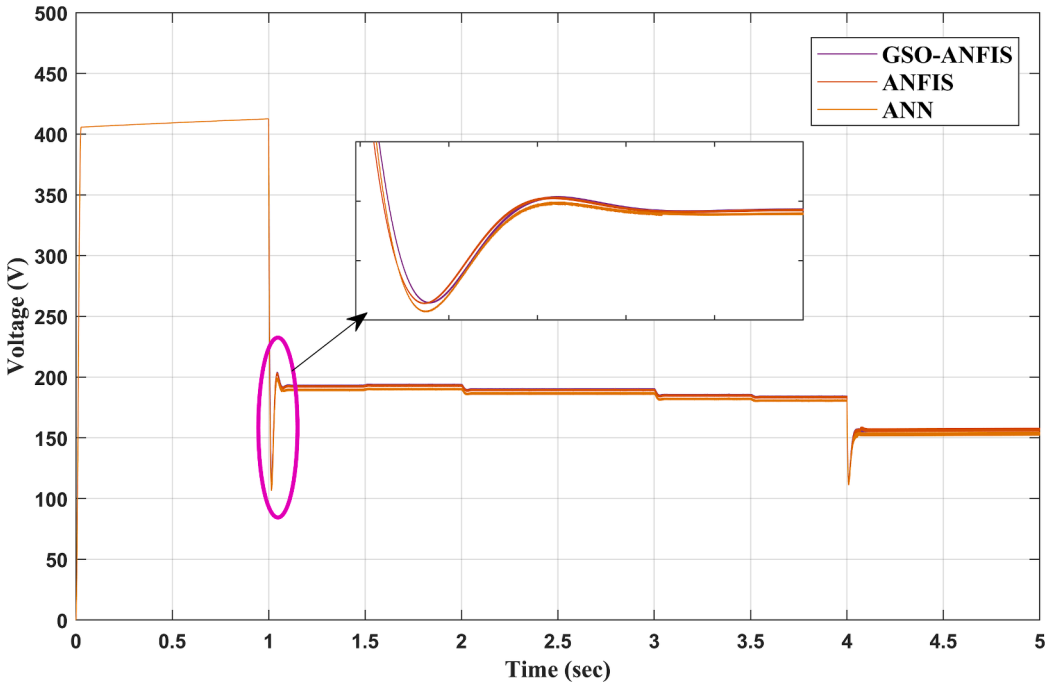

Fig. 18. Comparative analysis of voltage waveform of all the models under dynamic loading conditions.

current occurs at transient time instances t4 and t7 with the proposed model, measuring 0.389 and 0.305, respectively. The change in voltage has also been observed as 0.470 and 0.369. When compared with ANN and ANFIS, the proposed GSO-ANFIS model exhibits the least deviation during severe transient states.

4.2. Testing of PEMFC under dynamic variation of load

The dynamic variation of the load has been carried out to perform the efficiency valuation of the proposed technique with the fuel cell. Four different loads of both the combination of resistance and inductance have been connected in parallel with the switching arrangement. Seven switching transient pattern analysis has been carried out. Algorithm-2 presents the pseudo-code for GSO-ANFIS under dynamic loading conditions.

Algorithm 2: Pseudo Code for GSO-LSTM MPPT

Require: Initialize GSO parameter, μ, α, t_{sw}, load
Ensure: Ensure Duty Cycle $(D) \in GSO-ANFISset$
Begin, set input parameter, randomly choose the initial population
Repeat, Evaluate fitness value and MSE for each iteration
for each iteration $i \leqslant N$
Compute MSE and Duty Cycle D
if $D < 0.875$ **then**
Then start GSO-ANFIS

(*continued on next page*)

(*continued*)

Algorithm 2: Pseudo Code for GSO-LSTM MPPT

```
    For μ⩽0.88
      CASE-1 = Triangle MF = 7
  else
      CASE-2 = Sigmoid MF = 7
      Optimize the μ
  else
      D_set = D_old(0.88)
  end if
```

In order to verify the impact of dynamic loading both the P&O and INC-method have been tested for validation evaluation.

Table-8 and Table-9 shows the performance comparison of the proposed GSO-ANFIS and benchmarking model with both P&O and INC methods respectively under dynamic loading conditions. Here the MAE, RMSE, and other statistical parameters are on the higher side, this is because of the change in the loading pattern. However, the proposed algorithm again provides the best result in terms of accuracy rate as compared to other benchmarking models.

Fig. 17 represents a comparative analysis of the current waveform of all the models under varying loading conditions. As observed there is a reduction of 13.42% of current as compared to case-1. During the changeover operation of the loading pattern, a ripple content of ±17% has been noticed for ANN and that of ±11% has been observed for ANFIS. However, with GSO-ANFIS model it has been reduced to 9.24%. The proposed model also limits the variation up to 7-cycles of operation as prescribed by IEEE standard c.11–2017 and has been validated with international power quality standards also.

Similarly, Fig. 18 represents a comparative analysis of the voltage waveform of all the benchmarking models. A maximum overshoot of 4.93% has been noticed for transient condition which is 3.07% less as compared to an average range of benchmarking models. Table-10 shows a comparative analysis of different power quality issues in PEMFC limited to current and voltage magnitude only.

Here in Table-10, shows the deviation of di/dt and dv/dt alongwith % change in error. As observed, ANN with $L_1 + L_2 + L_3(L_1 - Load - 1, L_2 - Load - 2, L_3 - Load - 3)$ shows maximum %

Table 10
Comparative analysis of different power quality studies in PEMFC under dynamic loading condition.

Type of Algorithm	Loading Pattern	di/dt level	% change	dv/dt level	% change
ANN	L1	0.22	4.62	0.28	4.72
	L1 + L2	0.67	4.91	0.84	5.20
	L1 + L2 + L3	1.03	7.28	1.28	7.72
	L1 + L2 + L3 + L4	2.41	11.07	2.98	12.11
ANFIS	L1	0.24	4.57	0.31	4.67
	L1 + L2	0.73	4.72	0.91	5.04
	L1 + L2 + L3	1.00	6.84	1.24	7.27
	L1 + L2 + L3 + L4	2.16	9.83	2.67	10.76
GSO + ANFIS	L1	0.17	4.18	0.22	4.25
	L1 + L2	0.54	4.66	0.68	4.89
	L1 + L2 + L3	0.89	6.53	1.11	6.91
	L1 + L2 + L3 + L4	2.18	7.86	2.69	8.80

Table 11
Performance comparison among the models.

Sr. No.	Parameter	ANN	ANFIS	GSO-ANFIS
1	Transient Fluctuation	poor	moderate	good
2	Dynamic Response	poor	moderate	good
3	Steady Oscillation	moderate	moderate	moderate
4	Tracking Speed	poor	poor	moderate
5	Accuracy Level	80.33	86.51	89.97
6	Static Error	0.86	0.49	0.28
7	Tolerance Band	[0.1–0.27]	[0.16–0.62]	[0.11–0.87]
8	Power Conversion Efficiency	low	high	high
9	Convergence Time	NA	31 ms.	19 ms.

Table 12
Predictive performance analysis of P&O MPPT using different optimization Models

Sr. No.	Parameters	ANN (%)	ANFIS (%)	GSO-ANFIS (%)
1	+ Predictive Value	92.7	93.04	95.11
2	- Predictive Value	87.93	86.43	91.36
3	+ Likehood Ratio	23	23	22
4	- Likehood Ratio	0.6	0.48	0.66
5	Sensitivity	81.07	86.53	89.49
6	Specificity	92.08	93.17	94.15

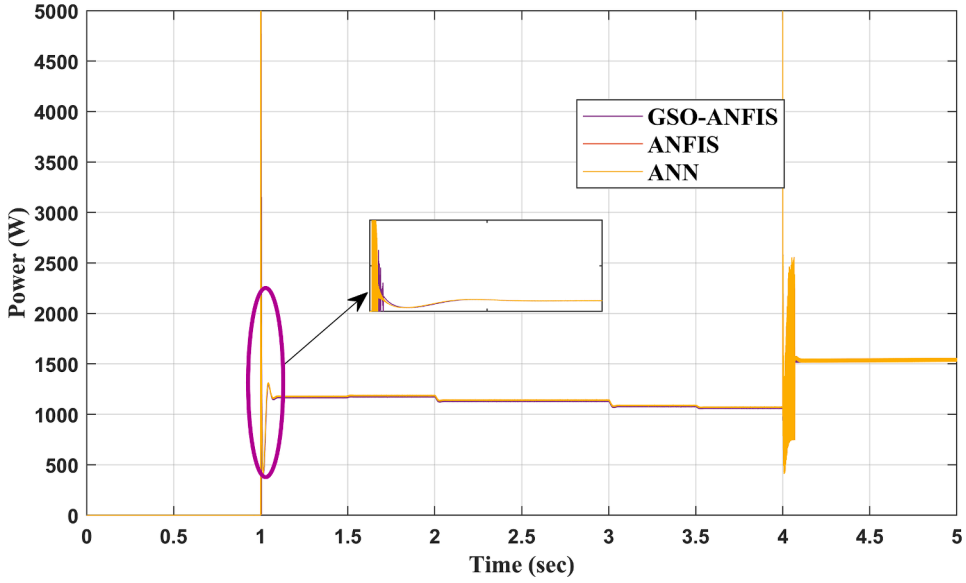

Fig. 19. Comparative analysis of power waveform of all the models under dynamic loading conditions.

change in di/dt rating of 7.28% as compared to ANFIS and GSO + ANFIS model. Similarly, GSO-ANFIS model with 4-loading pattern shows a voltage % change of 8.80 as compared to 12.11 for ANN and 10.76 for the ANFIS model.

Fig. 19, shows the power curve under dynamic loading conditions. As can be seen, the ANN-based P&O model exhibits a power overshoot from 1231 watts to 5004 watts, while the GSO + ANFIS model restricts it to 1328 watts. Additionally, the system presents a transient disturbance over a period of 0.07 s.

5. Discussion

Performance evaluation of different MPPT (Benchmarking model + GSO-ANFIS) has been carried out for static and dynamic loading conditions. Based on the experimental analysis, Table-11, represents the summarized comparative analysis of all the models and Table-12 shows the p&O MPPT using different optimization algorithms.

Under dynamic stability analysis, the proposed GSO-ANFIS model is more stable to change in load as compared to another benchmarking model. This is because the GSO is deciding the type and range of ANFIS membership function as compared to conventional ANFIS. There is not much difference in the steady-state oscillation of the proposed technique and to dynamic change in load. The accuracy level in terms of clear distinction among the transient intervals is 11.53% better with the proposed GSO + ANFIS model as compared to the ANNN model and 3.72% efficient as compared to the classical ANFIS model.

The tolerance band which determines the range of variation in dynamic load is quite large like [0.11–0.87]. This gives a wider range of operating characteristics to the hybrid controller. The timely dependent duty cycle also increases the power conversion efficiency of the controller. However, there is not much difference between the classical ANFIS model and the GSO-ANFIS model.

The statistical analysis of the three predictive models, namely ANN, ANFIS, and GSO-ANFIS, reveals compelling insights into their performance across key parameters. In terms of positive predictive value, GSO-ANFIS demonstrates remarkable accuracy at 95.11%, outperforming both ANN (92.7%) and ANFIS (93.04%). Similarly, GSO-ANFIS excels in negative predictive value, registering an impressive score of 91.36%, surpassing ANN (87.93%) and ANFIS (86.43%). The likelihood ratio, a critical measure of diagnostic accuracy, is notably higher for GSO-ANFIS at 0.66, indicating its enhanced ability to make correct predictions compared to ANN (0.6) and ANFIS (0.48). Moreover, GSO-ANFIS exhibits superior sensitivity (89.49%) and specificity (94.15%) in correctly identifying positive and negative outcomes, respectively, further underscoring its robust performance. These findings emphasize the GSO-ANFIS model's statistical superiority, positioning it as a highly effective tool for accurate prediction and optimization in the domain of PEMFC technology.

6. Conclusion

The present research paper introduces and tests an improved hybrid GSO-ANFIS MPPT model for PEMFC fuel cell applications under two different conditions: static and dynamic load. Two conventional MPPT algorithms, P&O and INC, were used for comparison. One of the most common power quality problems with the P&O model is that the operating point drifts due to changes in temperature and pressure. However, currently, available models of different MPPT techniques cannot track this variation in the conventional P&O method when there are dynamic changes in state. To address this issue, the present model considers an optimization algorithm along with ANFIS to ensure drift-free operation with the P&O MPPT model.

The proposed GSO-ANFIS model has been tested for a stand-alone load under static and dynamic loading conditions. In order to validate the GSO-ANFIS model, a detailed mathematical model along with operation has been developed and validated through the VI-curve of the MPPT for both temperature & pressure variation curves.

The performance of the proposed GSO-ANFIS model has been tested with both P&O and INC algorithms for efficiency evaluation. In the classical ANFIS model, the error between the input to output is ±0.34 whereas with the proposed GSO-ANFIS model it has been reduced to ± 0.07 around the mean position. The ANN model shows a sluggish response in tuning the P&O algorithm parameter. Therefore, the duty cycle variation to an instantaneous change in load does not get reflected in the system output. The neural network regression analysis shows that the proposed model is best fitted for R = 0.99877. This concludes that the power extracted from the fuel cells using the proposed algorithm is higher and linear as compared to ANN and ANFIS models.

CRediT authorship contribution statement

K Jyotheeswara Reddy: Conceptualization, Methodology, Software, Data curation, Writing - original draft, Visualization, Investigation. **Ritesh Dash:** Conceptualization, Methodology, Software, Data curation, Writing - original draft, Visualization, Investigation. **Vivekanandan Subburaj:** Conceptualization, Methodology, Software, Data curation, Writing - original draft, Visualization, Investigation. **B Hemanth Kumar:** Conceptualization, Methodology, Software, Data curation, Writing - original draft, Visualization, Investigation. **Dhanamjayulu C:** Supervision, Software, Validation, Writing - review & editing. **Frede Blaabjerg:** Supervision, Software, Validation, Writing - reviewing & editing, Funding. **SM Muyeen:** Supervision, Software, Validation, Writing - review & editing.

Declaration of Competing Interest

The authors declare that they have no known competing financial interests or personal relationships that could have appeared to influence the work reported in this paper.

Data availability

No data was used for the research described in the article.

References

[1] Olabi AG, Onumaegbu C, Wilberforce T, Ramadan M, Abdelkareem MA, Al-Alami AH. Critical review of energy storage systems. Energy 2021;214:118987.
[2] Olabi AG. Renewable energy and energy storage systems. Energy 2017;136:1–6.
[3] Inci M. Interline fuel cell (I-FC) system with dual-functional control capability. Int J Hydrogen Energy 2020;45(1):891–903.
[4] Zhong D, Lin R, Liu D, Cai X. Structure optimization of anode parallel flow field for local starvation of proton exchange membrane fuel cell. J Power Sources 2018;403:1–10.
[5] Wang C, Nehrir MH, Shaw SR. Dynamic models and model validation for PEM fuel cells using electrical circuits. IEEE Trans Energy Conversion 2005;20(2):442–51.
[6] Karthikeyan V, Das PV, Blaabjerg F. Implementation of MPPT control in fuel cell fed high step up ratio DC-DC converter. In: 2018 2nd IEEE International Conference on Power Electronics, Intelligent Control and Energy Systems (ICPEICES); 2018. p. 689–93.
[7] Benyahia N, Denoun H, Badji A, Zaouia M, Rekioua T, Benamrouche N, Rekioua D. MPPT controller for an interleaved boost dc-dc converter used in fuel cell electric vehicles. Int J Hydrogen Energy 2014;39(27):15196–205.
[8] Rezk H, Fathy A. Performance improvement of PEM fuel cell using variable step-size incremental resistance MPPT technique. Sustainability 2020;12(14):5601.
[9] Harrag A, Messalti S. Variable step size IC MPPT controller for PEMFC power system improving static and dynamic performances. Fuel Cells 2017;17(6):816–24.
[10] Mohamed AP, Chandrakala KV, Saravanan S, November. Comparative study of maximum power point tracking techniques for fuel cell powered electric vehicle. In IOP Conference Series: Materials Science and Engineering (Vol. 577, No. 1, 2019. p. 012031).
[11] Chen PY, Yu KN, Yau HT, Li JT, Liao CK. A novel variable step size fractional order incremental conductance algorithm to maximize power tracking of fuel cells. Appl Math Model 2017;45:1067–75.
[12] Harrag A, Messalti S. How fuzzy logic can improve PEM fuel cell MPPT performances? Int J Hydrogen Energy 2018;43(1):537–50.
[13] Rezk H, Aly M, Fathy A. A novel strategy based on recent equilibrium optimizer to enhance the performance of PEM fuel cell system through optimized fuzzy logic MPPT. Energy 2021;234:121267.

[14] Reddy KJ, Sudhakar N. A new RBFN based MPPT controller for grid-connected PEMFC system with high step-up three-phase IBC. Int J Hydrogen Energy 2018;43(37):17835–48.
[15] Reddy KJ, Sudhakar N. High voltage gain interleaved boost converter with neural network based MPPT controller for fuel cell based electric vehicle applications. Ieee Access 2018;6:3899–908.
[16] Srinivasan S, Tiwari R, Krishnamoorthy M, Lalitha MP, Raj KK. Neural network based MPPT control with reconfigured quadratic boost converter for fuel cell application. Int J Hydrogen Energy 2021;46(9):6709–19.
[17] Savrun MM, İnci M. Adaptive neuro-fuzzy inference system combined with genetic algorithm to improve power extraction capability in fuel cell applications. J Cleaner Prod 2021;299:126944.
[18] Reddy KJ, Sudhakar N. ANFIS-MPPT control algorithm for a PEMFC system used in electric vehicle applications. Int J Hydrogen Energy 2019;44(29):15355–69.
[19] Padmanaban S, Priyadarshi N, Bhaskar MS, Holm-Nielsen JB, Hossain E, Azam F. A hybrid photovoltaic-fuel cell for grid integration with jaya-based maximum power point tracking: experimental performance evaluation. IEEE Access 2019;7:82978–90.
[20] Ahmadi S, Abdi S, Kakavand M. Maximum power point tracking of a proton exchange membrane fuel cell system using PSO-PID controller. Int J Hydrogen Energy 2017;42(32):20430–43.
[21] Rana KPS, Kumar V, Sehgal N, George S. A novel dPdI feedback based control scheme using GWO tuned PID controller for efficient MPPT of PEM fuel cell. ISA Trans 2019;93:312–24.
[22] Fathy A, Abdelkareem MA, Olabi AG, Rezk H. A novel strategy based on salp swarm algorithm for extracting the maximum power of proton exchange membrane fuel cell. Int J Hydrogen Energy 2021;46(8):6087–99.
[23] Kumar S, Shaw B. Design of off-grid fuel cell by implementing ALO optimized PID-based MPPT controller. In: Soft Computing in Data Analytics; 2019. p. 83–93.
[24] Shaw B. Comparison of SCA-optimized PID and P&O-based MPPT for an off-grid fuel cell system. In: Soft computing in data analytics; 2019. p. 51–8.
[25] Nasiri Avanaki I, Sarvi M. A new maximum power point tracking method for PEM fuel cells based on water cycle algorithm. J Renew Energy Environ 2016;3(1):35–42.
[26] Priyadarshi N, Sharma AK, Azam F. A hybrid firefly-asymmetrical fuzzy logic controller based MPPT for PV-wind-fuel grid integration. Int J Renew Energy Res (IJRER) 2017;7(4):1546–60.
[27] Bayat P, Baghramian A. A novel self-tuning type-2 fuzzy maximum power point tracking technique for efficiency enhancement of fuel cell based battery chargers. Int J Hydrogen Energy 2020;45(43):23275–93.
[28] Sisworahardjo NS, Yalcinoz T, El-Sharkh MY, Alam MS. Neural network model of 100 W portable PEM fuel cell and experimental verification. Int J Hydrogen Energy 2010;35(17):9104–9.
[29] İnci M, Caliskan A. Performance enhancement of energy extraction capability for fuel cell implementations with improved Cuckoo search algorithm. Int J Hydrogen Energy 2020;45(19):11309–20.
[30] Ge X, Ahmed FW, Rezvani A, Aljojo N, Samad S, Foong LK. Implementation of a novel hybrid BAT-Fuzzy controller based MPPT for grid-connected PV-battery system. Control Eng Practice 2020;98:104380.
[31] Reddy J, Sudhakar N. Design and analysis of a hybrid PV-PEMFC system with MPPT controller for a three-phase grid-connected system. J Green Eng 2018;8(2):151–76.
[32] Reddy KJ, Sudhakar N, Saravanan S, Babu BC. High step-up boost converter with neural network based MPPT controller for a PEMFC power source used in vehicular applications. Int J Emerg Electr Power Syst 2018;19(5).